



# The formation of Laurentia: Evidence from shear wave splitting



Mitch V. Liddell<sup>a,\*</sup>, Ian Bastow<sup>a</sup>, Fiona Darbyshire<sup>b</sup>, Amy Gilligan<sup>c</sup>, Stephen Pugh<sup>a</sup>

<sup>a</sup> Imperial College London, United Kingdom

<sup>b</sup> Université du Québec à Montréal, Canada

<sup>c</sup> University of Aberdeen, Scotland, United Kingdom

## ARTICLE INFO

### Article history:

Received 1 April 2017

Received in revised form 5 September 2017

Accepted 12 September 2017

Available online 3 October 2017

Editor: P. Shearer

### Keywords:

shear wave splitting

Paleoproterozoic

seismic anisotropy

Trans-Hudson orogen

Laurentia

cratons

## ABSTRACT

The northern Hudson Bay region in Canada comprises several Archean cratonic nuclei, assembled by a number of Paleoproterozoic orogenies including the Trans-Hudson Orogen (THO) and the Rinkian–Nagssugtoqidian Orogen. Recent debate has focused on the extent to which these orogens have modern analogues such as the Himalayan–Karakoram–Tibet Orogen. Further, the structure of the lithospheric mantle beneath the Hudson Strait and southern Baffin Island is potentially indicative of Paleoproterozoic underthrusting of the Superior plate beneath the Churchill collage. Also in question is whether the Laurentian cratonic root is stratified, with a fast, depleted, Archean core underlain by a slower, younger, thermally-accreted layer. Plate-scale process that create structures such as these are expected to manifest as measurable fossil seismic anisotropic fabrics. We investigate these problems via shear wave splitting, and present the most comprehensive study to date of mantle seismic anisotropy in northern Laurentia. Strong evidence is presented for multiple layers of anisotropy beneath Archean zones, consistent with the episodic development model of stratified cratonic keels. We also show that southern Baffin Island is underlain by dipping anisotropic fabric, where underthrusting of the Superior plate beneath the Churchill has previously been interpreted. This provides direct evidence of subduction-related deformation at 1.8 Ga, implying that the THO developed with modern plate-tectonic style interactions.

© 2017 The Author(s). Published by Elsevier B.V. This is an open access article under the CC BY license (<http://creativecommons.org/licenses/by/4.0/>).

## 1. Overview

The geological record of the northern Hudson Bay region in Canada exceeds 2 billion years, including several Archean nuclei and a series of Paleoproterozoic orogens that culminated in the assembly of the cratonic core of North America, Laurentia. The largest of these is the Trans-Hudson Orogen (THO), which marks the ~1.8 Ga collision between the Archean Superior craton and the Churchill plate (Fig. 1; Hoffman, 1988). Structural and thermobarometric studies suggest the THO was similar in scale and style to the modern-day Himalayan–Karakoram–Tibet Orogen (HKTO) (e.g., St-Onge et al., 2006), a finding corroborated by seismic studies of the crust (Thompson et al., 2010; Pawlak et al., 2011; Gilligan et al., 2016), and recently by the discovery of low-temperature, high-pressure eclogite rocks within the THO indicative of plate-scale subduction (Weller and St-Onge, 2017). Farther north are the remnants of the 1.7 Ga Nagssugtoqidian Orogen (NO; Fig. 1) which records the collision of the North Atlantic, Superior, and Rae cratons with plate-scale deformation distinct from that imparted

from the nearly contemporaneous THO to the south. Laurentia is also characterised by one of the deepest lithospheric roots ('keels') on Earth, with the lithospheric mantle reaching depths >280 km in places (e.g., Bao and Eaton, 2015; Porritt et al., 2015). Recent debate has centred on whether the root is stratified, with a seismically fast, depleted, upper layer underlain by a younger, slower, thermal lithosphere (e.g., Yuan and Romanowicz, 2010), and whether such a layer is restricted to Archean domains or extends beneath Proterozoic regions as well (e.g., Darbyshire et al., 2013).

Increasing our knowledge of the seismic structure of the Hudson Bay region is central to our understanding of the assembly of Laurentia. Modern-style plate tectonics would have imparted measurable, plate-scale, seismically-anisotropic fossil fabrics in the lithosphere. For example, plate-scale underthrusting of the Superior lithosphere beneath the Churchill plate could be expected to create dipping anisotropic layers with fast directions perpendicular to the direction of collision, while keel stratification should result in multiple layers of anisotropy (e.g., Yuan and Romanowicz, 2010; Darbyshire et al., 2013).

When a radially-polarised shear wave encounters seismically anisotropic media, it will split into two orthogonal shear waves polarised along the fast and slow axes of the material. The splitting

\* Corresponding author.

E-mail address: [m.liddell14@imperial.ac.uk](mailto:m.liddell14@imperial.ac.uk) (M.V. Liddell).

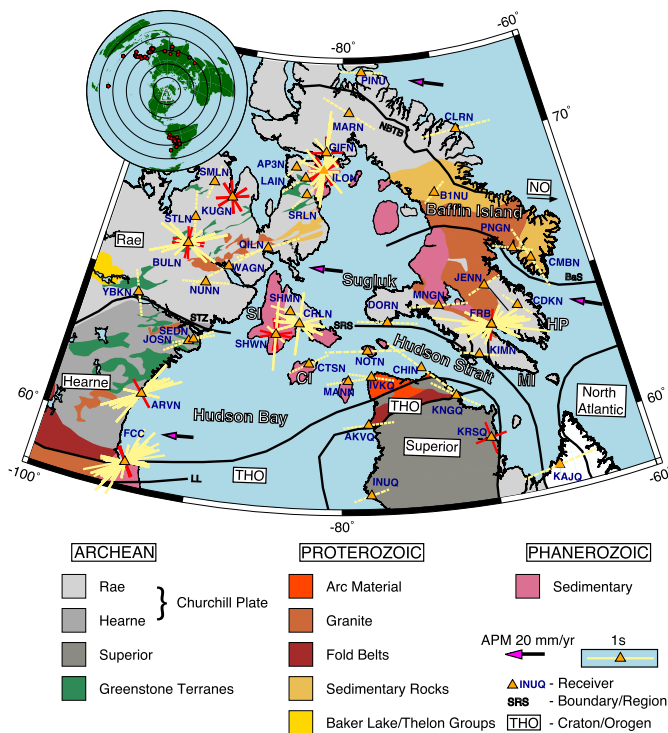


**Fig. 1.** Geological map of northern Hudson Bay with SKS splitting results. Dashed yellow bars indicate stacked  $\phi$  and  $\delta t$  values, solid yellow bars indicate unstacked individual measurements. Red bars are null measurements with  $90^\circ$  ambiguity. Absolute plate motion arrows are purple. The inset global map shows the location of the receiver network, the red dots are earthquakes used in this study. BaS, Baffin Suture; CI, Coats Island; HP, Hall Peninsula; MI, Meta-Incognita; SI, Southampton Island; SRS, Soper River Suture; STZ, Snowbird Tectonic Zone; THO, Trans-Hudson Orogen; NBTB, Northeast Baffin Thrust Belt; NO, Nagssugtoqidian Orogen; LL, Lynn Lake Fault; MISH, Meta-Incognita-Sugluk-Hall-Peninsula. (For interpretation of the references to colour in this figure, the reader is referred to the web version of this article.)

parameters  $\phi$  (the polarisation direction of the fast shear wave) and  $\delta t$  (the delay time between the two waves) can then be used to characterise the crust and mantle anisotropy beneath the receiver (Silver and Chan, 1991).

Here we present the results of a shear wave splitting study of SKS and SKKS (hereafter referred to as SKS) phases recorded by 43 seismograph stations in the northern Hudson Bay region. Regional SKS splitting studies often utilise only 1–2 yr of data, limiting the backazimuthal coverage of high-quality measurements, and precluding the possibility of interpreting more complicated dipping or multi-layer structures. However, our data set comprises stations with recording times between 4 and 23 yr. The Hudson Bay Lithospheric Experiment (HuBLE; e.g., Bastow et al., 2011) stations in the Hudson Strait and on Baffin Island were active from 2007 to 2011. The Portable Observatories for Lithospheric Analysis and Research Investigating Seismicity (POLARIS; Eaton et al., 2005) network began deployment in 2004 in western Hudson Bay and northern Quebec. Stations FCC and FRB from the Canadian National Seismograph Network have been active since 1994.

## 2. Tectonic background

Our study region contains large portions of 3 Archean provinces (Rae, Hearne, Superior; Fig. 1) that comprise much of the Canadian Shield (Hoffman, 1988). The nuclei of these Archean regions are thought to have originally grown by lateral accretion and wedging of proto-continents in a pre-subduction setting (Snyder et al., 2016). The Rae and Hearne are divided by the Snowbird Tectonic Zone (STZ), potentially a 1.9 Ga collision zone (Berman et al., 2007), and together comprise the bulk of the Churchill plate.

The Churchill–Superior collision is thought to have been complex, trapping several smaller micro-plates between the principal cratons before terminal collision at 1.8 Ga (Corrigan et al., 2009). Southern Baffin Island has been postulated to be an amalgamation of some of these micro-continents, including the Meta-Incognita (MI) block, the Sugluk block, and the Hall Peninsula block, together dubbed the ‘MISH’ block (Snyder et al., 2013). The Baffin Suture (St-Onge et al., 2006) marks the boundary between the southeast Rae craton and the Meta-Incognita (MI) microcontinent that makes up much of southern Baffin Island. The northward trending features and relatively shallow burial depth of the region indicate that Meta-Incognita was the upper plate in the Rae–MI collision (Corrigan et al., 2009).

Northern Baffin Island includes the western extension of Greenland’s Paleoproterozoic Rinkian fold belt along the SE–NW oriented Northeast Baffin Thrust Belt (NBTB; Fig. 1), which exerted southwesterly pressure and strikes roughly perpendicular to the structural deformation patterns to the south, overprinting several Archean and Paleoproterozoic provinces (Jackson and Berman, 2000). This generally north–south striking fold belt has been linked to the east–west oriented plate-scale Nagssugtoqidian Orogen (NO) of southern Greenland (e.g., Connelly et al., 2006). The combined Rinkian–Nagssugtoqidian orogen is similarly asymmetric, and potentially similar in scale, to the THO to the south.

## 3. SKS splitting with cluster analysis

Seismic anisotropy refers to the directional dependence of seismic wavespeed. When a shear wave encounters an anisotropic medium, it will split into two shear waves, orthogonally polarised, one travelling faster than the other (e.g., Silver and Chan, 1991). The polarisation direction ( $\phi$ ) of the fast shear wave, and the delay time ( $\delta t$ ) between them can be used to characterise the seismic anisotropy of the material. P-to-S converted phases such as SKS and SKKS, are ideally-suited for upper-mantle shear-wave splitting studies; they are radially polarised at the core–mantle boundary and thus record no source-side anisotropy (e.g. Silver and Chan, 1991; Long and Silver, 2009). Olivine, the most common mineral in Earth’s upper mantle, is highly anisotropic. A crystallographic preferred orientation (CPO) may develop in the olivine in response to strain, with its  $a$ -axis aligned parallel to the direction of flow (e.g. Bystricky et al., 2000; Tommasi et al., 2000; Zhang and Karato, 1995), assuming steady-state, one dimensional shear flow (Kaminski and Ribe, 2002). The shear wave splitting parameters,  $\phi$  and  $\delta t$ , can therefore be related to pre-existing ‘fossil’ anisotropy in the lithosphere (e.g. Silver and Chan, 1991; Vauchez and Nicolas, 1991), mantle convection patterns (e.g. Vinnik et al., 1989), absolute plate motion directions (e.g. Debayle and Ricard, 2013), aligned melt/fluid (e.g., Blackman and Kendall, 1997), or any combination thereof.

We inspected SKS phases for earthquakes of  $m_b \geq 6$  occurring at epicentral distances of  $\geq 88^\circ$  from 2004 to 2017. For permanent stations FRB and FCC, our search extended back to 1993. In total 5483 event–station pairs were processed, and 406 were included in the final dataset. Data were filtered prior to analysis using a zero-phase Butterworth bandpass filter with corner frequencies 0.04 and 0.3 Hz. Splitting parameters were constrained using the semi-automated approach of Teanby et al. (2004), built on the Silver and Chan (1991) method. Horizontal components are rotated and time-shifted to minimise the second eigenvalue of the covariance matrix for particle motion within a time window around the shear wave arrival. This is equivalent to linearising the particle motion and minimising tangential component shear wave energy. If the particle motion is linearised initially this is called a ‘null’ measurement and indicates that the anisotropic fast direction

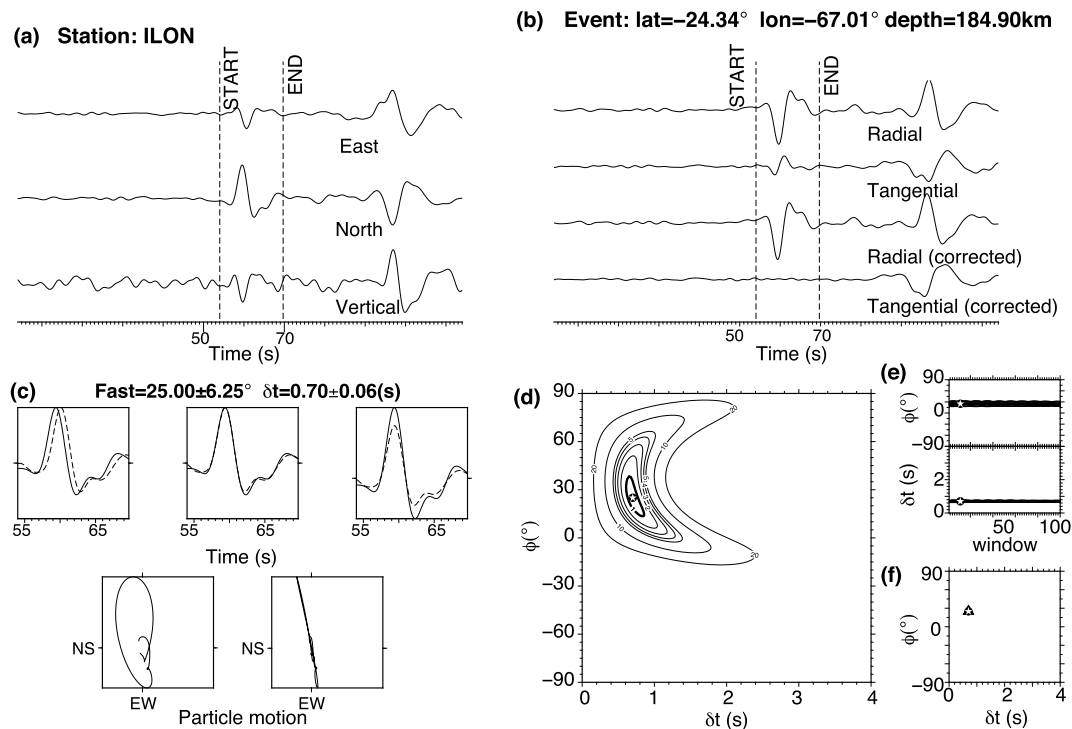


**Fig. 2.** High-quality splitting measurement example from station ILLON. (a) The recorded seismogram showing the SKS phase and the initial window. (b) The seismogram rotated into radial and tangential components both before (top two) and after (bottom two) processing. (c) Top L–R: close up of the SKS phases for the fast and slow waveforms before correction, after correction, and after correction without normalised amplitudes. Bottom L–R: particle motion before and after correction. (d) Contour map showing stability of the splitting parameters. Lines indicate one standard deviation. The thick line indicates 95 per cent confidence. (e) Splitting parameter variations as a function of the changing window. (f) Cluster analysis results for  $\phi$  and  $\delta t$  for each of the 100 windows. These values were very stable over the full range of windows.

is either perpendicular or parallel to the backazimuth of the wave, or that no anisotropic material was encountered. Null measurements therefore have an inherent  $90^\circ$  ambiguity, and are reported in Fig. 1 as a red cross. The Silver and Chan (1991) approach takes a single, manually picked, shear-wave analysis window. In the cluster analysis approach of Teanby et al. (2004), however, the splitting analysis is performed for a range of window lengths and cluster analysis is utilised to find measurements that are stable over many different windows. All splitting parameters were determined after analysis of 100 different windows. An example of the analysis is shown in Fig. 2.

#### 4. SKS splitting results

The results obtained for SKS splitting in northern Canada displayed visually in Fig. 1 are summarised in Table 1; a full list of all splitting results and associated errors is included in supplemental materials. The average signal to noise ratio (as defined by Restivo and Helffrich, 1999) for these data is 15.5 with a standard deviation of 7.1. Quality control was enforced by visual inspection of each split to ensure linearisation of the particle motion. We also enforced data error upper limits of  $\pm 15^\circ$  in  $\phi$  and  $\pm 0.5$  s in  $\delta t$ , although most were much lower (see supplemental materials for complete dataset). This is a much stricter limit than the previous study of Snyder et al. (2013), where errors sometimes exceeded  $\pm 30^\circ$  in  $\phi$  and 2 s in  $\delta t$ . Where relevant, a model class is assigned to each station to describes the first order type of anisotropy observed at that station (Table 1). Each basic class of model (single layer, two-layer, dipping layer) has a distinctive backazimuthal pattern in their splitting parameters. A dipping anisotropic layer will vary relatively smoothly with  $360^\circ$  periodicity. An anisotropic model of a vertical interface has  $180^\circ$  backazimuthal periodicity, and a two-layer model has  $90^\circ$  periodicity (Fig. 3; Silver and Savage, 1994). A dipping model has peak-to-peak  $\phi$  variations  $\leq 90^\circ$ ,

as opposed to interfaces or two-layer models, which have sharper changes in  $\phi$  and peak-to-peak variations approaching  $180^\circ$ .

The model-class for each station in Table 1 is chosen to be the simplest possible that explains the observations. For many of the stations in Fig. 1 a single, horizontal anisotropic layer could adequately explain the data. Data from such stations were stacked using a procedure based on the method of Wolfe and Silver (1998) to obtain single pairs of splitting parameters (e.g., CTSN, DORN, MARN, in Fig. 1; Table 1). We cannot, however, preclude the possibility that this assumption is invalid for stations where backazimuthal coverage of earthquakes is insufficient to resolve more complex dipping or multi-layer patterns of anisotropy (e.g., Silver and Savage, 1994). Plots of  $\phi$  vs backazimuth for each station in Fig. 1 are in the supplemental materials. For stations that exhibited clear variation typical of a more complex anisotropic structure, a grid search of relevant model parameters was performed to forward model the  $\phi$  and  $\delta t$  using the MSAT toolkit of Walker and Wookey (2012), which is capable of modelling both multi-layer and dipping anisotropy. Bastow et al. (2011) suggested the presence of dipping anisotropy based on backazimuthal variation of splitting parameters; we are the first to explore this hypothesis quantitatively. The ‘N’ column in Table 1 compares the number of splits used to define each station in our dataset directly to that of Bastow et al. (2011), in brackets.

#### 5. Discussion

##### 5.1. Causes of observed anisotropy

Across our study area, we commonly observe  $\delta t \geq 1$  s (Fig. 1, Table 1), implying a mantle contribution to the observations: regional continental crust is  $\sim 40$  km thick and can only reasonably account for  $\delta t \leq 0.5$  s (Barruol and Mainprice, 1993; Silver, 1996). North American absolute plate motion (APM) is  $\sim 22$  mm/yr, well

**Table 1**

SKS splitting parameters for stacked (top) and unstacked (bottom) stations. Subscript values refer to backazimuth ranges for binned results, or the backazimuth of recording for null measurements.  $N$  is the number of splits (including nulls) for that station or backazimuthal range, bracketed numbers are the number of splits used by Bastow et al. (2011) for the same station. For unstacked results, bold type text indicates the first-order model class groups based on Fig. 3.

Station	$\phi$	$\delta t$	$N$	Station	$\phi$	$\delta t$	$N$
AKVQ	84 ± 4	0.9 ± 0.1	3	MANN	82 ± 1	0.8 ± 0.1	8 (2)
AP3N	43 ± 2	0.6 ± 0.1	10	MARN	-58 ± 1	1.1 ± 0.1	16
B1NU	47 ± 8	0.5 ± 0.1	3	MNGN	-88 ± 1	1.1 ± 0.1	23 (11)
CDKN	-47 ± 5	0.7 ± 0.1	4 (2)	MUMO	73 ± 1	1.3 ± 0.1	14
CHIN	-49 ± 3	1.6 ± 0.1	3	NOTN	90 ± 1	1.6 ± 0.1	8 (6)
CLRN	86 ± 5	1.3 ± 0.1	1	NUNN	84 ± 3	0.9 ± 0.1	3 (1)
CMBN	-20 ± 1	1.3 ± 0.2	2 (2)	PINU	-86 ± 2	0.8 ± 0.1	4
CTSN	63 ± 1	0.8 ± 0.1	13 (2)	PNGN	-71 ± 2	0.7 ± 0.1	6 (2)
DORN	-85 ± 3	1.1 ± 0.1	4 (3)	QILN	67 ± 1	1.2 ± 0.1	6 (2)
INUQ	71 ± 2	0.6 ± 0.1	5	SEDN	70 ± 1	0.8 ± 0.1	10
IVKQ	-80 ± 2	0.8 ± 0.1	2	SHMN	-77 ± 3	0.7 ± 0.1	5 (2)
JENN	69 ± 14	0.7 ± 0.2	1	SILO	62 ± 1	0.6 ± 0.1	7
JOSN	59 ± 5	1.0 ± 0.1	2	SMLN	14 ± 4	0.6 ± 0.1	2
KASO	91 ± 2	1.1 ± 0.1	4	SRLN	44 ± 1	0.7 ± 0.1	5
KAJQ	-71 ± 8	0.3 ± 0.1	2	STLN	-9 ± 2	1.0 ± 0.1	3
KIMN	-76 ± 2	0.7 ± 0.1	6 (3)	VIMO	83 ± 1	0.6 ± 0.1	9
KJKQ	51 ± 2	0.7 ± 0.1	7	WAGN	54 ± 1	1.5 ± 0.1	8 (2)
KNGQ	-58 ± 2	1.1 ± 0.1	5	YBKN	-27 ± 5.25	0.3 ± 0.1	4
LAIN	56 ± 2	1.0 ± 0.1	7				
<b>Multiple</b>				ILON <sub>300–360</sub>	140 ± 5	1.1 ± 0.2	1
ARVN <sub>0–90</sub>	46 ± 4	1.1 ± 0.09	1	ILON <sub>2</sub>	null	-	2
ARVN <sub>90–180</sub>	29 ± 5	1.5 ± 0.10	1	ILON <sub>290</sub>	null	-	3
ARVN <sub>180–275</sub>	45 ± 2	0.8 ± 0.02	7	ILON <sub>316</sub>	null	-	-
ARVN <sub>275–300</sub>	61 ± 5	0.9 ± 0.04	1	ILON <sub>327</sub>	null	-	-
ARVN <sub>300–315</sub>	-89 ± 9	0.7 ± 0.06	1	ILON <sub>330</sub>	null	-	2
ARVN <sub>315–360</sub>	59 ± 4	1.5 ± 0.09	2	ILON <sub>334</sub>	null	-	3
ARVN <sub>320</sub>	null	-	2	SHWN <sub>90–180</sub>	0 ± 4	1.4 ± 0.1	1
BULN <sub>90–275</sub>	56 ± 6	1.0 ± 0.10	5 (2)	SHWN <sub>180–360</sub>	128 ± 9	0.5 ± 0.1	1
BULN <sub>275–360</sub>	114 ± 7	0.9 ± 0.20	6 (-)	SHWN <sub>282</sub>	null	-	-
FCC <sub>0–90</sub>	55 ± 4	0.9 ± 0.1	2	SHWN <sub>259</sub>	null	-	-
FCC <sub>90–180</sub>	2 ± 10	0.7 ± 0.1	2	<b>Dipping</b>			
FCC <sub>180–275</sub>	41 ± 1	0.8 ± 0.1	29	FRB <sub>0–90</sub>	126 ± 2	1.1 ± 0.1	3 (-)
FCC <sub>275–300</sub>	77 ± 6	0.6 ± 0.1	2	FRB <sub>90–183</sub>	52 ± 8	0.6 ± 0.1	3 (1)
FCC <sub>300–315</sub>	90 ± 4	0.9 ± 0.1	5	FRB <sub>183–270</sub>	62 ± 7	0.9 ± 0.1	3 (2)
FCC <sub>315–360</sub>	41 ± 1	0.8 ± 0.1	6	FRB <sub>270–300</sub>	83 ± 1	0.9 ± 0.1	19 (10)
FCC <sub>316</sub>	null	-	-	FRB <sub>300–330</sub>	103 ± 2	0.7 ± 0.1	9 (6)
FCC <sub>320</sub>	null	-	3	FRB <sub>330–360</sub>	107 ± 4	0.7 ± 0.1	5 (1)
FCC <sub>325</sub>	null	-	3	HP <sub>0–90</sub>	123 ± 1	1.3 ± 0.1	5
FCC <sub>327</sub>	null	-	-	HP <sub>90–180</sub>	70 ± 18	0.6 ± 0.2	3
<b>Interface</b>				HP <sub>180–270</sub>	77 ± 4	0.9 ± 0.1	3
CRLN <sub>110–180</sub>	5 ± 7	1.2 ± 0.20	1 (2)	HP <sub>270–300</sub>	84 ± 1	0.9 ± 0.1	21
CRLN <sub>300–360</sub>	97 ± 11	0.8 ± 0.50	9 (1)	HP <sub>300–330</sub>	99 ± 2	0.8 ± 0.1	18
GIFN <sub>90–180</sub>	7 ± 5	1.3 ± 0.2	4	HP <sub>330–360</sub>	102 ± 2	0.8 ± 0.1	19
GIFN <sub>180–360</sub>	140 ± 4	0.7 ± 0.1	1	<b>Null Only</b>			
GIFN <sub>269</sub>	null	-	-	KUGN <sub>258</sub>	null	-	2
ILON <sub>90–180</sub>	30 ± 2	0.8 ± 0.1	8	KUGN <sub>319</sub>	null	-	-
ILON <sub>180–300</sub>	106 ± 4	0.9 ± 0.1	3	KRSQ <sub>346</sub>	null	-	-

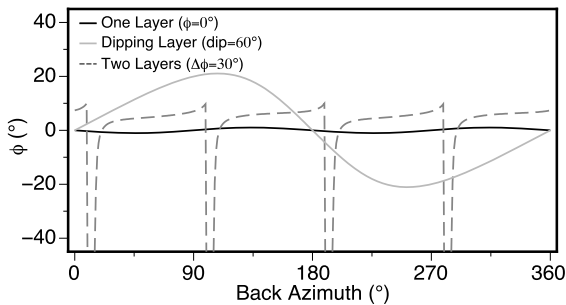


**Fig. 3.** MSAT calculated  $\phi$  responses for three basic classes of anisotropy.  $\Delta\phi$  indicates difference in fast direction between layers. Layer thickness and alignment fraction of olivine  $a$ -axis does not affect the patterns.

below the  $\sim 40$  mm/yr sometimes considered a minimum for basal drag fabric development (e.g., Debayle and Ricard, 2013; Martin-

Short et al., 2015). We observe no consistent, network-wide alignment with the current APM direction, which has been relatively constant for the past  $\sim 50$  Myr (Müller et al., 2016). Although we cannot preclude the possibility that older basal drag fabrics exist beneath the region, asthenospheric fabrics due to APM or regional mantle flow (e.g., Forte et al., 2015) would, according to Fresnel Zone arguments (Alsina and Snieder, 1995), be expected to produce only gradual variations in  $\phi$  and  $\delta t$  across our network. Our observed splitting parameters, in fact, vary over horizontal length-scales as  $\sim 150$  km (e.g., Southampton Island stations versus CTSN, Fig. 6). We therefore reject APM as an interpretation for our observed anisotropy, as opposed to Snyder et al. (2013) who interpreted APM as contributing a lower layer of anisotropy across the entirety of the Hudson Bay region. The paucity of tectonic activity since  $\sim 1.8$  Ga rules out aligned melt as a plausible cause of the observed anisotropy, so our discussion proceeds on the assumption that our data are primarily sensitive to fossil lithospheric

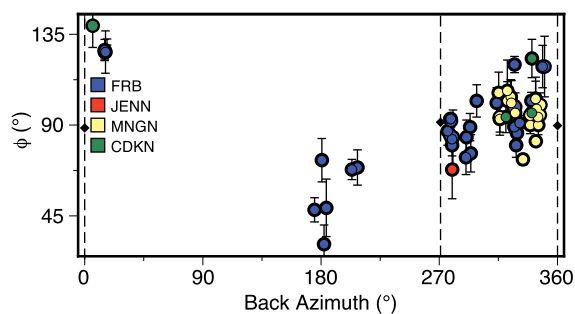


**Fig. 4.** Splitting parameters for HP block stations on southern Baffin Island (Fig. 1). Null measurements are indicated by dashed lines with diamonds at the parallel/perpendicular to backazimuth points.

anisotropy, consistent with earlier studies of the region (Bastow et al., 2011).

Several stations in Table 1 exhibit strong backazimuthal variation in splitting parameters, implying the presence of complex structure, including multiple and/or dipping anisotropic layers. We address these issues in the following sections on a region-by-region basis.

### 5.2. Evidence for proterozoic plate-scale underthrusting Beneath Baffin Island

Fast directions for stations in the Hudson Strait and along the northern coast of Quebec and southern coast of Baffin Island tend to parallel the strike of the THO (Fig. 1; Stations AKVQ, MANN, CTSN, IVKQ, NOTN, DORN, CHIN, KIMN, KNGQ). This interpretation is supported by the general trend in anisotropic direction found by Darbyshire et al. (2013) using surface waves, and the earlier SKS splitting study of Bastow et al. (2011). Unfortunately, the easternmost stations, KRSQ and KAJQ, had very few successful splits and so cannot be used to confirm or refute the THO hypothesis. Lithospheric-scale THO deformation clearly exerts first-order control on the anisotropy. The approximately EW fast direction of PNGN parallels the Baffin suture to the west of the station. At CMBN,  $\phi$  aligns more closely with the SE turn of the suture. At station PNGN,  $\phi$  parallels the APM direction, but the short length scale change compared to station CMBN, less than 100 km away, suggests strongly that the source of the anisotropy is more likely within the ~200 km-thick lithosphere in this region (Alsina and Snieder, 1995; Porritt et al., 2015).

Stations FRB, CDKN, JENN, and MNGN lie within the Hall Peninsula. To first order,  $\phi$  at MNGN and CDKN parallels the trace of the THO, but JENN is nearly perpendicular (Fig. 1). The reason for this becomes clear in Fig. 4; JENN records a split from a backazimuth not sampled by CDKN or MNGN, but mirrors observations at FRB at similar backazimuths (Fig. 4), giving credence to the idea that these stations sample similar structure and warrant consideration as a composite ‘Hall Peninsula’ or ‘HP’ station with good backazimuthal coverage. The stations included in the ‘HP’ stack were chosen based on their proximity to FRB (which provides most of the data and backazimuthal coverage to the stack) and because they share similar local geology. The Hall Peninsula region (Fig. 1) is characterised by high grade metamorphism, and was part of the leading edge of the Churchill plate during the THO (St-Onge et al., 2006, 2009). Nearby stations KIMN and DORN are not included in the HP group because KIMN lies on the other side of the Soper River suture from the rest of the stations, and DORN has lower grade metamorphism on the western reaches of Baffin Island. The splitting parameters for all HP stations were stacked within appropriate backazimuth bins (Table 1, Fig. 5), revealing a clear, smoothly-varying 360° periodicity, without the sharp changes in  $\phi$  that are characteristic of multi-layer anisotropy (Fig. 3). There-

fore, that class of model was used to initialise an MSAT modelling procedure to characterise the anisotropic structure.

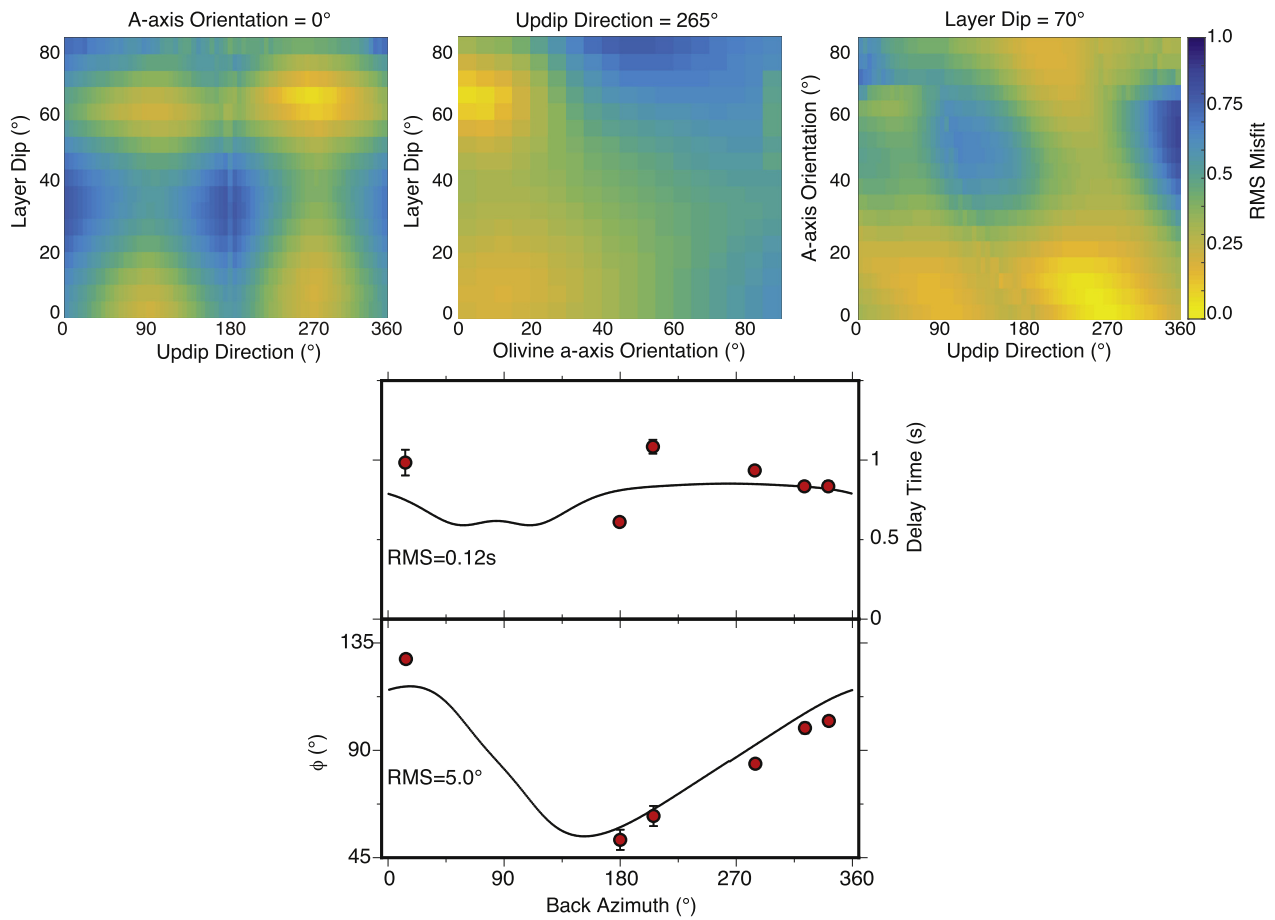
A grid search varying layer dip, up-dip direction, and olivine a-axis azimuth (AAZ) orientation was performed and the root mean squared (RMS) misfit between the model response for each set of parameters and the amalgam HP station data was calculated to indicate the agreement between model and observations. RMS was calculated using the formula:  $RMS = \sqrt{\frac{1}{n}(x_1^2 + x_2^2 \dots x_n^2)}$  where  $n$  is the number of observed data points, and  $x$  is the difference between the data point and the modelled curve, less the error. Data points were assumed to have errors in backazimuth of  $\pm 5^\circ$ . The best fitting model was determined by the lowest combined RMS for both for  $\phi$  and  $\delta t$ . The RMS values for each splitting parameter were normalised for each cell in the grid search, then combined (Fig. 5, top) such that the maximum value in each grid is 1. This method ensures that both  $\phi$  and  $\delta t$  are included in the determination of the best fitting model parameters.

Fig. 5 shows the results of the grid search for the three model parameters. Initially, AAZ =  $0^\circ$  (aligned with the dip direction), the simplest possible scenario. The minimum RMS value gives an updip direction of  $265^\circ \pm 10^\circ$  and a dip angle of  $70^\circ \pm 5^\circ$ . These values are then held constant while varying the other two parameters to confirm the best fitting model values. The middle and right RMS surfaces in Fig. 5 confirm that an AAZ of  $0^\circ$  is appropriate. The best fitting model is therefore a layer dipping at  $70^\circ$ , with a dip direction of N85°E (updip direction of  $265^\circ$ ). These parameters yield an RMS of  $5.0^\circ$  and  $0.12$  s, for  $\phi$  and  $\delta t$ , respectively. Layer thickness and olivine alignment fraction had no effect on the pattern of the splitting parameters; the effect was limited to a static shift of  $\delta t$ , and is therefore not well defined. What can be confidently concluded is that SKS splitting resolves a significant amount of eastward dipping anisotropy beneath southern Baffin Island. Such a dipping layer is consistent with recent findings of eclogite rocks in the THO indicative of deep plate-scale subduction (Weller and St-Onge, 2017). Our HP block results therefore provide compelling support for the hypothesis that the Superior plate underthrust the Churchill plate in a modern-style plate tectonic collision at  $\sim 1.8$  Ga.

### 5.3. Evidence for lithospheric subdivisions: implications for the two-plate THO hypothesis

Splitting parameters for stations on Southampton Island (SI) are clearly distinguished from the nearby Hudson Strait stations:  $\phi$  varies sharply between  $315^\circ$  and  $180^\circ$  backazimuth at stations CRLN, SHWN, and SHMN, while CTSN can be explained easily by a single, horizontal anisotropic layer (Fig. 6). With no data points at backazimuths  $\leq 180^\circ$ , we cannot confidently determine the precise anisotropic model that would best explain the observations. However, we can discount some possibilities by observing that the smoothly varying  $\phi$  over  $180^\circ$  backazimuth (Fig. 6) is uncharacteristic of a two-layer model (which has a periodicity of  $90^\circ$ ); peak-to-peak variations of  $\phi$  ( $\sim 135^\circ$ ) are larger than expected ( $\leq 90^\circ$ ) for a dipping layer (Figs. 3, 5). Further, the low metamorphic grade of Southampton Island rocks indicates that SI has not undergone the same deformation and uplift as the higher-grade rocks on southern Baffin Island (St-Onge et al., 2009). Superior plate underthrusting, and a dipping layer, is therefore less likely in this region.

A more plausible explanation for the Southampton Island observations could be lateral variations in anisotropy due to a nearby terrane boundary. This interpretation is in line with magnetoteluric evidence of a thickening resistive crust to the northeast of Southampton Island, which was interpreted as a potential terrane boundary by Spratt et al. (2012). Such a boundary could potentially



**Fig. 5.** (Top) Normalised RMS misfit surfaces for  $\phi$  and  $\delta t$  combined. Left surface sets olivine  $a$ -axis to  $0^\circ$  relative to dip direction. The parameters with lowest RMS misfit are each kept constant individually in the next two surfaces. (Bottom) Modelled response for the best fitting dip,  $a$ -axis orientation, and up-dip direction plotted against stacked HP block splitting parameters.

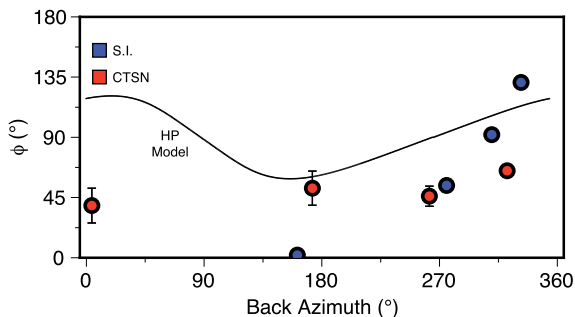


**Fig. 6.** Splitting parameters for the stacked Southampton Island stations and nearby CTSN, in Hudson Strait. Both groups are stacked in backazimuth bins:  $0\text{--}90^\circ$ ,  $90\text{--}180^\circ$ ,  $180\text{--}285^\circ$ ,  $285\text{--}330^\circ$ , and  $330\text{--}360^\circ$ . Solid black line is the best fitting HP model from Fig. 5.

be an extension of the Rae-Hearne boundary (Snowbird Tectonic Zone; Fig. 1), or an extension of the MISH block beneath this region. Similar  $V_p/V_s$  ratios and metasedimentary rocks between SI and mainland Rae (Thompson et al., 2010) support the former, while geological models by Corrigan et al. (2009) support the latter.

While the nature of the boundary cannot be confirmed from our data, the extension of the STZ onto Southampton Island is less likely than an influence from the MISH block because of the similarity in  $\phi$  between the Rae and the Hearne on the mainland (Fig. 1). Stations NUNN, WAGN, and QILN on the Rae mainland, and SEDN and JOSN on the Hearne (Fig. 1), parallel THO-related deformation rather than the SI pattern shown in Fig. 6. Therefore,

Southampton Island is anisotropically distinct both from the cratonic provinces (Rae/Hearne) to the north and the Hudson Strait to the south. This strongly suggests that Southampton Island is part of a lithospheric block separate from the Superior or the Churchill plates. Our observations in this region thus imply that the THO cannot be considered as a simple two-plate Proterozoic collision.

#### 5.4. Northerly extent of the THO on Melville Peninsula

The north-central Rae domain is dominated by granite-greenstone rocks with Paleoproterozoic deformation zones, potentially having been reworked by far-field THO pressure (Carson et al., 2004). With the notable exception of station BULN, the stations on the central Rae craton in Fig. 1 parallel these surface structural trends. The average anisotropic fast direction for the Melville Peninsula stations LAIN, AP3N, and SRLN, is  $34^\circ$ , the same orientation found for mantle-depth geoelectric strike by Spratt et al. (2013) (Fig. 7). Studies by Berman et al. (2005) and Corrigan et al. (2009) also noted strong NE-SW geological trends in this regions, and related them to late-Archean events followed by THO related deformation. Stations MARN and PINU on northern Baffin Island display  $\phi$  values that parallel the Northeast Baffin Thrust Belt (Jackson and Berman, 2000), which is the western extent of the Nagssugtoqidian orogen (NO) preserved in modern-day Greenland.

ILON and GIFN (Fig. 8) have strongly varying fast direction, however, we do not present any modelling of these stations because of the lack of reliable results from the  $0\text{--}180^\circ$  backazimuth. The peak-to-peak variation of  $\phi$  for IILON/GIFN in Fig. 8 precludes

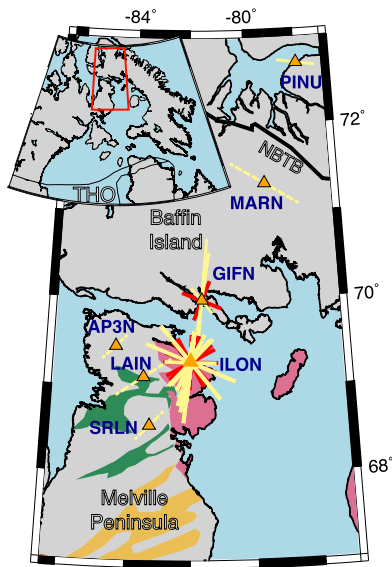


**Fig. 7.** Geological map of Melville Peninsula and northern Baffin Island with SKS splitting results. Dashed yellow bars indicate stacked  $\phi$  and  $\delta t$  values, solid yellow bars indicate unstacked individual measurements with 90° ambiguity. Legend is the same as Fig. 1. THO, Trans-Hudson Orogen; NBTB, Northeast Baffin Thrust Belt. (For interpretation of the references to colour in this figure legend, the reader is referred to the web version of this article.)

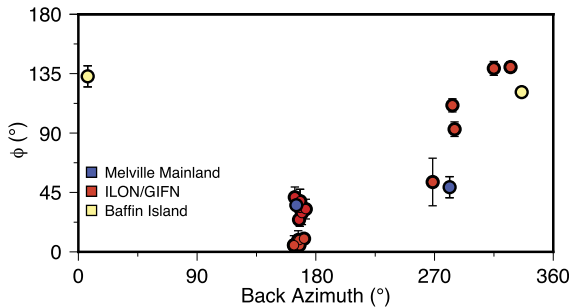


**Fig. 8.** Fast direction as a function of backazimuth showing similarities between GIFN/ILO and two single-layer-interpreted regions at different backazimuths. Mainland Melville stations are AP3N/LAIN/SRLN. Baffin Island stations are MARN/PINU.

the possibility of a dipping layer, and the data are not 90° periodic as expected for two-layer systems (Fig. 3). Although we cannot preclude the possibility that multi-layer anisotropy exists here, our data coverage limits us to discussion of the variable  $\phi$ , and comparison with nearby, less variable, stations. Stations GIFN and ILO lie between the two orogen-dominated regions and display variable  $\phi$  values that show influence from both (Fig. 8). At southerly backazimuths,  $\phi$  values are close to those observed on the mainland of Melville Peninsula, but significantly change to parallel the Baffin Island stations as backazimuth increases to ~300° (Fig. 8). These stations represent a transect through deformation regimes, and therefore mark the approximate limit of Proterozoic deformation both from the south and the north. It is expected that orogenies of the size of the THO and the NO will overprint any previous anisotropic signature. This is consistent with the view that fossil lithospheric anisotropy documents the last major tectonic event in a region (Silver and Chan, 1991). This has been previously interpreted for Melville Peninsula near ILO and GIFN (Spratt et al., 2013; Berman et al., 2005). Our results indicate a THO-related deformation zone ~700 km wide, similar to the width of  $\geq 650$  km suggested by Gilligan et al. (2016) across the northern Quebec-southern Baffin transect, and comparable to the 400–1000 km width of the modern-day Tibetan plateau.

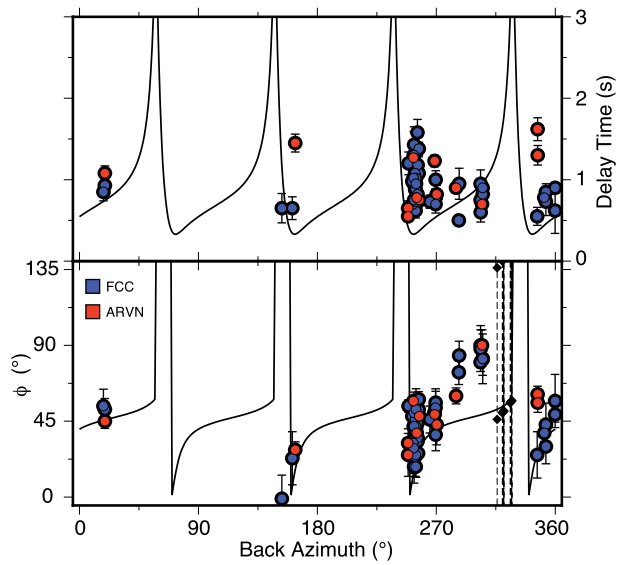


**Fig. 9.** Fast direction and delay time as a function of back azimuth for both Western Hudson Bay stations. Null measurements are dashed lines with diamonds at the parallel/perpendicular to backazimuth points. The similarity is such that the same structure can be interpreted beneath each station. The black line is a 2-layer model with a 50 km thick upper layer with  $\phi = 31^\circ$  over an 80 km thick layer with  $\phi = 79^\circ$ .

### 5.5. Implications for 2-stage keel formation

Western Hudson Bay stations FCC and ARVN have wide back-azimuthal coverage and similar variations in  $\phi$  and  $\delta t$  (Fig. 9). For both stations  $\phi$  varies from ~45° to ~20° but increases sharply around 270° backazimuth to ~90°. This pattern most closely resembles the 90° periodicity of the 2-layer synthetic model in Fig. 3. Station BULN has a similar, but less clear, pattern of splitting parameters. It potentially warrants discussion as a multi-layer model also, but a relatively simple 2-layer system is not capable of recreating the observations. The cratonic nucleus of the Rae province grew by accreting terranes to its boundaries (Snyder et al., 2016). The variability of  $\phi$  observed at BULN, which lies on one of these accreted terranes, could be from complex anisotropic fabrics that are the remains of these Archean-age accretionary processes, but nearby stations lack the backazimuthal coverage to corroborate this interpretation.

Snyder et al. (2013) published receiver function results and anisotropic  $\phi$  values for a two-layer system for station FCC (Table 2 and Fig. 8 of Snyder et al., 2013). We used the receiver functions to define potential layer thicknesses for their  $\phi$  values and created a model with which to compare our data. This model has a  $\phi$  of 31° overlying 79°, with layer depths of 50 km and 130 km and is plotted as the solid line in Fig. 9. The model periodicity qualitatively fits our data and supports the interpretation of 2-layer anisotropy in this region. At backazimuths of ~315°, however, the data are less well matched, indicating that the model may be too simplistic. More recently published results from Darbyshire et al. (2013) show that the lithosphere–asthenosphere boundary in this region is at ~240 km depth; a value much deeper than the lower anisotropic layer used to produce the model in Fig. 9. Further, the similarity between the FCC and ARVN data in Fig. 9 links the structure beneath these stations, thus precluding the Lynn Lake fault (local to station FCC) from being the upper layer of anisotropy. A layered lithosphere model resulting from episodic cratonic development thus fits the observations better than one requiring APM.

Cratonic regions are typically underlain with exceptionally thick (~250 km) high wavespeed lithospheric keels. The highly-depleted cratonic core obtains a thermally accreted, more fertile boundary

layer at some point after initial cratonic development, probably no earlier than the Paleoproterozoic (Yuan and Romanowicz, 2010; Bastow et al., 2013; Bao et al., 2016; Boyce et al., 2016). Support for this interpretation comes from studies such as Yuan et al. (2011) and Darbyshire et al. (2013), which have found evidence for a stratified lithosphere, cratonic and otherwise, in North America using SKS splitting, long-period seismic wave inversion, and surface wave tomography. A variety of receiver function and SKS splitting studies have also suggested the presence of a sharp change in seismic velocity at mid-lithospheric depths in North America (e.g., Miller and Eaton, 2010; Yuan and Romanowicz, 2010). While our results do not support a simple two-layer model for this region, they are consistent with the presence of multiple layers exhibiting complex anisotropy and are therefore consistent with the presence of an MLD predicted by the two-stage cratonic development theory.

## 6. Conclusions

We have investigated seismic anisotropy across much of the northern Hudson Bay and Baffin Island region of Canada using shear-wave splitting analysis of up to 23 yr of SKS and SKKS phases. Below the Archean western coast of Hudson Bay we find strong evidence for at least two anisotropic layers in the lithosphere. Our observations are interpreted to be due to cratonic stratification and support a multi-stage keel development theory (e.g., Yuan and Romanowicz, 2010). More broadly across the study area, however, we observe a prevalence of anisotropic fast polarisation directions that parallel the strike of the Paleoproterozoic Trans Hudson Orogen (THO), implying that it imparted plate-scale anisotropic fabrics on the region at  $\sim 1.8$  Ga. Variations in  $\phi$  on Southampton Island reveal a unique mantle anisotropy signature consistent with the presence of a micro-continent (Meta-Incognita) caught between the colliding Churchill and Superior plates. This points to a more complex model than a simple two-plate system for the THO. The periodicity of  $\phi$  and  $\delta t$  for stations on southern Baffin Island indicates the presence of dipping anisotropy. We interpret the anisotropy to be due to the Superior plate underthrusting the Churchill at  $\sim 1.8$  Ga. THO-parallel plate-scale anisotropic fabrics persist as far north as Melville Peninsula, implying THO deformation was as laterally extensive ( $\sim 700$  km) as in the Himalayas today. Our results thus constitute strong evidence that modern-style plate tectonics were in action during, and were responsible for, Paleoproterozoic orogens.

## Acknowledgements

The authors would like to thank A. Walker for invaluable help understanding the MSAT forward modelling code, as well as A. Boyce, L. Petrescu, and C. Ogden of the ICratons group for numerous enlightening conversations about Canadian Precambrian geology and beyond. M.V. Liddell is funded by an Imperial College President's Scholarship. F.A. Darbyshire is supported by the Natural Sciences and Environment Research Council of Canada through their Discovery Grant and Canada Research Chair programmes (341802-2013-RGPIN).

## Appendix A. Supplementary material

Supplementary material related to this article can be found online at <https://doi.org/10.1016/j.epsl.2017.09.030>.

## References

- Alsina, D., Snieder, R., 1995. Small-scale sublithospheric continental mantle deformation: constraints from SKS splitting observations. *J. Geophys. Res.* 115 (9), 1–24.
- Bao, X., Eaton, D.W., 2015. Large variations in lithospheric thickness of western Laurentia: tectonic inheritance or collisional reworking? *Precambrian Res.* 266, 579–586.
- Bao, X., Eaton, D.W., Gu, Y.J., 2016. Rayleigh wave azimuthally anisotropic phase velocity maps beneath western Canada. *J. Geophys. Res.* 121, 1821–1834.
- Barruol, G., Mainprice, D., 1993. A quantitative evaluation of the contribution of crustal rocks to the shear-wave splitting of teleseismic SKS waves. *Phys. Earth Planet. Inter.* 78 (3–4), 281–300.
- Bastow, I.D., Thompson, David A., Wookey, J., Kendall, J.M., Helffrich, G., Snyder, D.B., Eaton, D.W., Darbyshire, F.A., 2011. Precambrian plate tectonics: seismic evidence from Northern Hudson Bay, Canada. *Geology* 39 (1), 91–94.
- Bastow, I.D., Eaton, D.W., Kendall, J.M., Helffrich, G.R., Snyder, D.B., Thompson, D.A., Wookey, J., Darbyshire, F., Pawlak, A.E., 2013. The Hudson Bay Lithospheric Experiment (HuBLE): insights into Precambrian plate tectonics and the development of mantle keels. *Geol. Soc. (Lond.) Spec. Publ.* 389 (1), 41–67.
- Berman, R.G., Davis, W., Pehrsson, S., 2007. Collisional Snowbird tectonic zone resurrected: growth of Laurentia during the 1.9 Ga accretionary phase of the Hudsonian orogeny. *Geology* 35 (10), 911–914.
- Berman, R.G., Sanborn-Barrie, M., Stern, R.A., Carson, C.J., 2005. Tectonometamorphism at ca. 2.35 and 1.85 Ga in the Rae domain, western Churchill province, Nunavut, Canada: insights from the structural, metamorphic and in situ geochronological analysis of the southwestern Committee Bay belt. *Can. Mineral.* 43 (1), 409–442.
- Blackman, D., Kendall, J.M., 1997. Sensitivity of teleseismic body waves to mineral texture and melt in the mantle beneath a midocean ridge. *Philos. Trans. R. Soc. A* 355, 217–231.
- Boyce, A., Bastow, I.D., Darbyshire, F., Ellwood, A.G., Gilligan, A., Menke, W., 2016. Subduction Beneath Laurentia modified the North American Craton Edge: evidence from P and S-wave tomography. *J. Geophys. Res.* 121, 5013–5030.
- Bystricky, M., Kunze, K., Burlini, L., Burg, J.-P., 2000. High shear strain of olivine aggregates: rheological and seismic consequences. *Science* 290, 1564–1567.
- Carson, C.J., Berman, R.G., Stern, R.A., Sanborn-Barrie, M., Skulski, T., Sandeman, H.A., 2004. Age constraints on the Paleoproterozoic tectonometamorphic history of the Committee Bay region, western Churchill Province, Canada: evidence from zircon and in situ monazite SHRIMP geochronology. *Can. J. Earth Sci.* 41 (9), 1049–1076.
- Connelly, J., Thrane, K., Krawiec, A., Garde, A., 2006. Linking the Palaeoproterozoic Nagsugtoqidian and Rinkian orogens through the Disko Bugt region of West Greenland. *J. Geol. Soc.* 163 (2), 319–335.
- Corrigan, D., Pehrsson, S., Wodicka, N., De Kemp, E.A., 2009. The Palaeoproterozoic Trans-Hudson Orogen: a prototype of modern accretionary processes. *Geol. Soc. (Lond.) Spec. Publ.* 327, 457–479.
- Darbyshire, F., Eaton, D.W., Bastow, I.D., 2013. Seismic imaging of the lithosphere beneath Hudson Bay: episodic growth of the Laurentian mantle keel. *Earth Planet. Sci. Lett.* 373, 179–193.
- Debayle, E., Ricard, Y., 2013. Seismic observations of large-scale deformation at the bottom of fast-moving plates. *Earth Planet. Sci. Lett.* 376, 165–177.
- Eaton, D.W., Adams, J., Asudeh, I., Atkinson, G.M., Bostock, M.G., Cassidy, J.F., Ferguson, I.J., Samson, C., Snyder, D.B., Tiampo, K.F., Unsworth, M.J., 2005. Investigating Canada's Lithosphere and earthquake hazards with portable arrays. *Eos Trans. AGU* 86 (17), 169.
- Forté, A.M., Simmons, N.A., Grand, S.P., 2015. Constraints on 3-D seismic models from global geodynamic observables: implications for the global mantle convective flow. In: Romanowicz, B., Dziewonski, A.M. (Eds.), 2nd edition. In: *Treatise on Geophys.*, vol. 1. Elsevier, Amsterdam, pp. 853–907.
- Gilligan, A., Bastow, I.D., Darbyshire, F., 2016. Seismological structure of the 1.8 Ga Trans-Hudson Orogen of North America. *Geochem. Geophys. Geosyst.* 17, 2421–2433.
- Hoffman, P.F., 1988. United Plates of America, the birth of a craton: Early Proterozoic assembly and growth of Laurentia. *Annu. Rev. Earth Planet. Sci.* 16 (1), 543–603.
- Jackson, G.D., Berman, R.G., 2000. Precambrian metamorphic and tectonic evolution of Northern Baffin Island, Nunavut, Canada. *Can. Mineral.* 38, 399–421.
- Kaminski, É., Ribe, N.M., 2002. Timescales for the evolution of seismic anisotropy in mantle flow. *Geochem. Geophys. Geosyst.* 3 (8), 1–17.
- Long, M.D., Silver, P.G., 2009. Shear wave splitting and mantle anisotropy: measurements, interpretations, and new directions. *Surv. Geophys.* 30 (4–5), 407–461.
- Martin-Short, R.A., Richard, M., Bastow, I.D., Totten, E., Richards, M., 2015. Mantle flow geometry from ridge to trench beneath the Gorda – Juan de Fuca plate system. *Nat. Geosci.* 8, 1–21.
- Miller, M.S., Eaton, D.W., 2010. Formation of cratonic mantle keels by arc accretion: evidence from S receiver functions. *Geophys. Res. Lett.* 37 (18), 1–5.
- Müller, R.D., Seton, M., Zahirovic, S., Williams, S.E., Matthews, K.J., Wright, N.M., Shephard, G.E., Maloney, K.T., Barnett-Moore, N., Bower, D.J., Cannon, J.S., 2016. Ocean basin evolution and global-scale reorganization events since Pangea breakup. *Annu. Rev. Earth Planet. Sci. Lett.* 44, 107–138.
- Pawlak, A., Eaton, D., Bastow, I., Kendall, J.-M., Helffrich, G., Wookey, J., Snyder, D., 2011. Crustal structure beneath Hudson Bay from ambient noise tomography: implications for basin formation. *Geophys. J. Int.* 184 (1), 65–82.
- Porritt, R.W., Miller, M.S., Darbyshire, F., 2015. Lithospheric architecture beneath Hudson Bay. *Geochem. Geophys. Geosyst.* 16 (7), 2262–2275.



- Restivo, A., Helffrich, G., 1999. Teleseismic shear wave splitting measurements in noisy environments. *Geophys. J. Int.* 137 (3), 821–830.
- Silver, P.G., 1996. Seismic anisotropy beneath the continents: probing the depths of geology. *Annu. Rev. Earth Planet. Sci.* 24 (1), 385–432.
- Silver, P.G., Chan, W.W., 1991. Shear wave splitting and subcontinental mantle deformation. *J. Geophys. Res.* 96 (B10), 16429–16454.
- Silver, P.G., Savage, M.K., 1994. The interpretation of shear-wave splitting parameters in the presence of two anisotropic layers. *Geophys. J. Int.* 119, 949–963.
- Snyder, D.B., Berman, R.G., Kendall, J.M., Sanborn-Barrie, M., 2013. Seismic anisotropy and mantle structure of the Rae craton, central Canada, from joint interpretation of SKS splitting and receiver functions. *Precambrian Res.* 232, 189–208.
- Snyder, D.B., Humphreys, E., Graham Pearson, D., 2016. Construction and destruction of some North American cratons. *Tectonophysics* 694, 464–485.
- Spratt, J.E., Craven, J.A., Sanborn-Barrie, M., 2012. Southampton Island magnetotelluric survey: data acquisition and preliminary analysis. *Geol. Surv. Can. Open File* 6988, 39 pp.
- Spratt, J.E., Jones, A.G., Corrigan, D., Hogg, C., Canada, N.R., 2013. Lithospheric geometry beneath Melville Peninsula, Nunavut, revealed by deep-probing magnetotelluric surveying. *Curr. Res., Geol. Surv. Can.* 12, 14 pp.
- St-Onge, M.R., Searle, M.P., Wodicka, N., 2006. Trans-Hudson orogen of North America and Himalaya–Karakoram–Tibetan orogen of Asia: structural and thermal characteristics of the lower and upper plates. *Tectonics* 25 (4), 1–22.
- St-Onge, M.R., Van Gool, J.A.M., Garde, A., Scott, D.J., 2009. Correlation of Archaean and Palaeoproterozoic units between northeastern Canada and western Greenland: constraining the pre-collisional upper plate accretionary history of the Trans-Hudson orogen. *Geol. Soc. Lond., Spec. Pubs.* 318 (1), 193–235.
- Teanby, N., Kendall, J.-M., van der Baan, M., 2004. Automation of shear-wave splitting measurements using cluster analysis. *Bull. Seism. Soc. Am.* 94 (2), 453–463.
- Thompson, D.A., Bastow, I.D., Helffrich, G.R., Kendall, J.M., Wookey, J., Snyder, D.B., Eaton, D.W., 2010. Precambrian crustal evolution: seismic constraints from the Canadian Shield. *Earth Planet. Sci. Lett.* 297 (3–4), 655–666.
- Tommasi, A., Mainprice, D., Canoval, G., Chastel, Y., 2000. Viscoplastic self-consistent and equilibrium-based modeling of olivine lattice preferred orientations: implications for the upper mantle seismic anisotropy. *J. Geophys. Res.* 105 (B4), 7893–7908.
- Vauchez, A., Nicolas, A., 1991. Mountain building: strike-parallel motion and mantle anisotropy. *Tectonophysics* 185 (3–4), 183–201.
- Vinnik, L.P., Farra, V., Romanowicz, B., 1989. Azimuthal anisotropy in the Earth from observations of SKS at geoscope and NARS broadband stations. *Bull. Seism. Soc. Am.* 79 (5), 1542–1558.
- Walker, A.M., Wookey, J., 2012. Record of modern-style plate tectonics in the Palaeoproterozoic Trans-Hudson orogen. *Nature Geoscience* 10, 305–312.
- Weller, O., St-Onge, M.R., 2017. MSAT – a new toolkit for the analysis of elastic and seismic anisotropy. *Comput. and Geosci.* 49, 81–90.
- Wolfe, C.J., Silver, P.G., 1998. Seismic anisotropy of oceanic upper mantle: shear wave splitting methodologies and observations. *J. Geophys. Res.* 103 (B1), 749–771.
- Yuan, H., Romanowicz, B., 2010. Lithospheric layering in the North American craton. *Nature* 466, 1063–1068.
- Yuan, H., Romanowicz, B., Fischer, K.M., Abt, D.L., 2011. 3-D shear wave radially and azimuthally anisotropic velocity model of the North American upper mantle. *Geophys. J. Int.* 184 (3), 1237–1260.
- Zhang, S., Karato, S.I., 1995. Lattice preferred orientation of olivine aggregates deformed in simple shear. *Nature* 375, 774–777.